AIAA 2003-3175

Rotor Wake Vortex Definition Using 3C-PIV Measurements – Corrected for Vortex Orientation

Casey L. Burley, Thomas F. Brooks
NASA Langley Research Center
Hampton, VA

Berend van der Wall
Institute of Flight Systems
German Aerospace Center (DLR)
Braunschweig, Germany

Hughues Richard, Markus Raffel
Institute of Aerodynamics and Fluid Technique
German Aerospace Center (DLR)
Gottingen, Germany

Philippe Beaumier, Yves Delrieux
Office National D'Etudes et de Recherches Aerospatiales (ONERA)
Chatillon, France

Joon W. Lim, Yung H. Yu, Chee Tung
Aeroflightdynamics Directorate (AFDD)
US Army Aviation and Missile Command (AMCOM)
NASA Ames Research Center
Moffett Field, CA.

Kurt Pengel, Edzard Mercker
German-Dutch Wind Tunnel (DNW)
Noordoostpolder, The Netherlands

9th AIAA/CEAS
Aeroacoustics Conference
May 12-14, 2003 / Hilton Head, South Carolina

AIAA-2003-3175

Rotor Wake Vortex Definition Using 3C-PIV Measurements – Corrected for Vortex Orientation

Casey L. Burley, Thomas F. Brooks
NASA Langley Research Center
Hampton, VA

Berend van der Wall
Institute of Flight Systems
German Aerospace Center (DLR)
Braunschweig, Germany

Hughues Richard, Markus Raffel
Institute of Aerodynamics and Fluid Technique
German Aerospace Center (DLR)
Gottingen, Germany

Philippe Beaumier, Yves Delrieux
Office National D'Etudes et de Recherches Aerospatiales (ONERA)
Chatillon, France

Joon W. Lim, Yung H. Yu, Chee Tung
Aeroflightdynamics Directorate (AFDD)
US Army Aviation and Missile Command (AMCOM)
NASA Ames Research Center
Moffett Field, CA.

Kurt Pengel, Edzard Mercker
German-Dutch Wind Tunnel (DNW)
Noordoostpolder, The Netherlands

ABSTRACT

Three-component (3-C) particle image velocimetry (PIV) measurements, within the wake across a rotor disk plane, are used to determine wake vortex definitions important for BVI (Blade Vortex Interaction) and broadband noise prediction. This study is part of the HART II test program conducted using a 40 percent scale BO-105 helicopter main rotor in the German-Dutch Wind Tunnel (DNW). In this paper, measurements are presented of the wake vortex field over the advancing side of the rotor operating at a typical descent landing condition. The orientations of the vortex (tube) axes are found to have non-zero tilt angles with respect to the chosen PIV measurement cut planes, often on the order of 45 degrees. Methods for determining the orientation of the vortex axis and reorienting the measured PIV velocity maps (by rotation/projection) are presented. One method utilizes the vortex core axial velocity component, the other utilizes the swirl velocity components. Key vortex parameters such as vortex core size, strength, and core velocity distribution characteristics are determined from the reoriented PIV velocity maps. The results are compared with those determined from velocity maps that are not corrected for orientation. Knowledge of magnitudes and directions of the vortex axial and swirl velocity components as a function of streamwise location provide a basis for insight into the vortex evolution.

SYMBOLS

C	rotor blade chord, 0.121m
CV	center of vorticity in (x,y) plane, m
DNW	German-Dutch Wind tunnel
DLR	German Aerospace Center
HART	HHC Aeroacoustic Rotor Test
k	grid point indices
j	indices for instantaneous image
R	rotor radius, 2 m
r_C	vortex core radius, m
u,v,w	velocity components for x,y,z coordinates,m/s
V_T	rotor tip speed, (218 m/s)
$(x,y,z)_{TUN}$	windtunnel coordinate system: (x_{TUN} positive downstream, y_{TUN} positive starboard, z_{TUN} positive up).
x,y,z	PIV image frame (rotated and non-rotated) coordinates, m, Figs. 4 and 9.
$\Box_z, \Box_z, \Box_z$	direction cosines of the vortex axis wrt x,y,z axes, respectively, see Eq. 3
Γ	circulation within r_C, m/s^2
$\Box$	transformation matrix of direction cosines
$\Box_0$	vortex axis tilt angle, deg
$\Box$	blade azimuth, measured counter-clockwise with $\Box$=0 in the x_{TUN} direction, deg
$\Box_0$	vortex axis tilt-alignment angle, deg
$\Box_z$	vorticity component normal to x,y plane, s^{-1}

superscripts

ℓ	defined in tilted vortex s^{ℓ} coordinate system
0	defined in PIV cut-plane s^0 coordinate system

INTRODUCTION

Helicopter rotor noise and flow fields have been studied and measured intensely over the last several decades in order to understand and predict the noise generation process as well as determine methods for control and reduction. Rotor blade vortex interaction (BVI) noise has received much of the attention, since it can dominate the radiated noise field adversely affects community acceptance of rotorcraft (Refs. 1-4). In addition to BVI noise, rotor broadband noise (blade self noise and blade wake interaction (BWI) noise has also been shown to be significant and even dominate the radiated noise field for certain operating conditions, such as shallow climb (Refs. 5,6). Both the BVI and BWI result from the blade interacting with the rotor wake and its associated turbulent field. In order to further develop understanding of the physics behind these phenomena and advance prediction and noise reduction capabilities, accurate detailed knowledge of the wake is critical. This includes not only the geometry of the wake, but its overall structure (core size, strength, and outer spiral extent) and its evolution process from initial creation (rollup process) to full development within the vicinity of the rotating blades.

Advances in measurement techniques and digital cameras have allowed measurements of the rotor wake to become increasingly more attainable. Measurement systems such as LDV (Laser Doppler Velocimetry) and PIV (Particle Image Velocimetry) are now routinely used to acquire instantaneous velocity measurements over relatively large areas and volumes. Leishman, et al. (Refs. 7, 8), Han, et al. (Ref. 9), Coyne, et al. (Ref. 10), Bhagwat and Leishman (Refs. 11, 12), and Martin, et al. (Ref. 13) have measured the tip vortex generated by a one- and two-bladed rotor in hover using 3-D LDV. Mahalingam and Komerath (Ref. 14, 15) measured the tip vortex from a two-bladed rotor in forward flight, also with 3-D LDV. The swirl and axial velocity profiles of the tip vortex as it ages as well as derived parameters such as core size, strength, and turbulence quantities have been documented in detail. Heineck, et al. (Ref. 16) used 3-Component (3-C) PIV to examine the wake of 2-bladed rotor in hover for wake ages up to 270 degrees. The effect of vortex wander on determining core size from the measured data was presented. McAlister, et al. (Ref. 17) obtained 3-C PIV to study the wake of a hovering rotor and the effect of a turbulence-generating device attached to the tip of the blade. The size and strength of the tip vortex was significantly altered. Raffel, et al. (Ref. 18) compared 3-D LDV with 2-C PIV measurements taken at one rotor azimuth location where the vortex orientation was known. The advantages and differences of the measurement techniques for application to measuring rotor vortex properties were discussed. Recent experimental efforts in 3-C PIV measurements of wake vortices are reported by Burley, et al. (Ref. 19) for a rotor in forward flight. This was the first in-depth look at the data that is also the subject of the present paper. There, a number of vortex parameters were determined but without an evaluation of the vortex orientations (and their effects on determined parameters) with respect to the PIV measurement cut planes.

When examining the flow field from experimental measurements, the plane normal to the vortex axis is not known a priori and in addition may vary with time. Experimentalists, typically use whatever knowledge is available about the flow field to obtain measurements that are normal to the vortex axis or at some known orientation with respect to the vortex. Van der Wall examined the importance of correct orientation in determining vortex core properties (Ref. 20). From LLS (Laser Light Sheet) data he extracted the vortex axis inclination with respect to the LDV measurement line.

The LDV data was then transformed into a plane normal to the vortex axis, and the vortex properties (vorticity, vortex center, core radius, circulation, and axial velocity) were then determined. It was found that core sizes were significantly smaller when orientation was accounted for. Also the core velocities, specifically the axial component was better resolved once the data was transformed into the plane normal to the vortex axis. To accurately extract vortex properties from wake measurements it is important to know the orientation of the vortex with respect to the measurements.

In this paper, two original methods are presented for determining the orientation of the vortex axis with respect to the PIV cut plane. The two methods employ the flow velocity vector field of the PIV cut-plane to resolve vortex orientation. Specifically, one method uses the axial flow within the vortex core to determine its orientation. The other method uses the tangential (or spin) velocity within the vortex core to define its orientation. The methods are applied to the PIV measurements obtained on the advancing side of a model rotor. Vortex quantities, such as core size and strength are determined from the PIV vector distribution corrected for orientation. These vortex quantities are compared to those obtained using data not corrected for orientation (Ref. 19). The core size and strength are important and key parameters to current comprehensive rotorcraft prediction analysis and hence their accuracy is critical. In addition to vortex core size and strength, the axial velocity component of the vortex is determined and evaluated using the corrected data.

TEST DESCRIPTION

In 2001, a major international cooperative research program called HART II, for Higher-harmonic-control (HHC) Aeroacoustics Rotor Test II, (Ref. 21-23) was conducted within US/German and US/French Memoranda of Understanding, by researchers from the German DLR, the French ONERA, the Netherlands DNW, the US Army Aeroflightdynamics Directorate (AFDD), and NASA Langley. The objective of the test was to investigate the physics of BVI, broadband noise, and vibration reduction concepts with the HHC technology, and to generate a comprehensive experimental database for code development and validation. To accomplish these objectives, extensive 3-C PIV measurements of the rotor wake, along with acoustic directivity measurements, unsteady blade surface pressure measurements, and blade deformation measurements were obtained.

The HART II was conducted in the open-jet, anechoic test section of the Large Low-speed Facility (LLF) of the DNW, which has an exit nozzle of 8 m by 6 m that provides a 19m-long free jet with a low-turbulence potential core. The set-up for the PIV measurements is shown in Fig. 1. The rotor hub was located 7 m downstream from the nozzle exit and maintained at 0.915 m above the tunnel centerline. The rotor is a 40-percent, dynamically and Mach-scaled model of the Bo105 main rotor and operated in the counter clockwise direction. The model is 4 m in diameter and consists of four hingeless blades that have a precone of 2.5 degrees at the hub. The rectangular planform blades have a chord length of 0.121 m, NACA 23012 sections (with tabbed trailing edge), −8 degrees linear twist, and standard rectangular tips. For the HART II test, the rotor was operated at a nominal rpm of 1041, thrust coefficient $C_T = 0.0044$, hover tip speed of 218 m/s, and an advance ratio of 0.15, for a range of rotor angles and conditions with and without HHC. The non-HHC baseline condition considered here

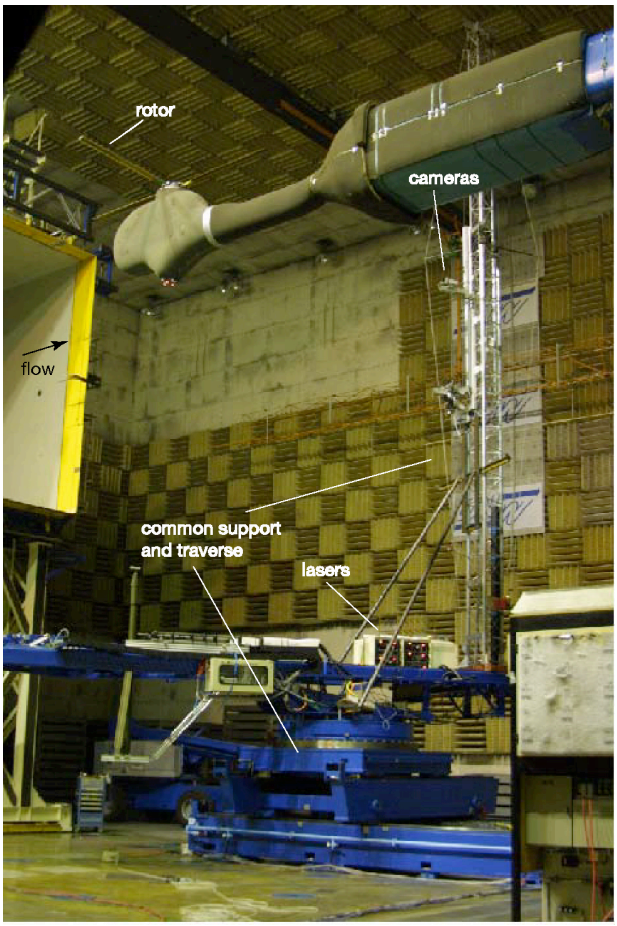

Figure 1. HART II rotor and 3-C PIV set-up in the DNW test section.

is for a rotor shaft angle of 5.3 degrees with respect to the tunnel axis. More detailed information on the rotor characteristics are given in Ref. 23.

3-C PIV Measurements

The PIV system implemented for this test consisted of five digital cameras and three double pulse Nd:YAG lasers with 2x320 mJ each. The lasers and cameras were mounted onto a common traversing system in order to keep the distance between the cameras and the light sheet constant while moving to different measurement locations within the rotor wake. Figure 1 shows rotor and traverse equipment in the DNW test section. The 5 cameras were located on the 15 m vertical tower; both above and below the rotor plane and the lasers are located underneath the rotor. Four of the cameras were for the 3-C PIV measurements. The fifth camera was used to visually check seeding prior to PIV data acquisition. To obtain measurements on the retreating side the entire support structure and tower was repositioned to the retreating side. Further details of the PIV systems are documented in Refs. 22-24.

Figure 2 shows the locations and orientations of the PIV measurement cut-planes over the rotor disk. To avoid blades being present in the PIV images, the data acquisitions were timed to different rotor positions for different wake-measurement coverage regions, In Figs. 2(a) and (b), this is indicated by a reference blade being alternately at ψ = 70 and 20 deg. Each black line segment represents a region where sets of 100 or more instantaneous PIV images were obtained. The PIV cut-planes were oriented at 30.7 deg. with respect to x_{TUN} for all measurement locations. A larger angle would have been desirable in order to be roughly normal to the vortex axes. But, this was not attainable due to orientation and distance requirements of the traversing rig. Based on pretest predictions, it was estimated that tilt angles of the vortices with respect to the cut lines on the outer part of the disk would be off axis as much as 30 to 45 deg. It will be seen in this report that up to 60 deg. was measured.

The testing procedure was designed to measure the wake from the same blade at all cut-plane locations indicated in Fig. 2. This would allow for the tip vortex to be investigated in detail from its creation through its evolution as it convects and traverses downstream throughout the rotor disk region. Because of this, any questions of blade-to-blade differences could be avoided. Further details of the measurement systems and process can be found in Refs. 22-24.

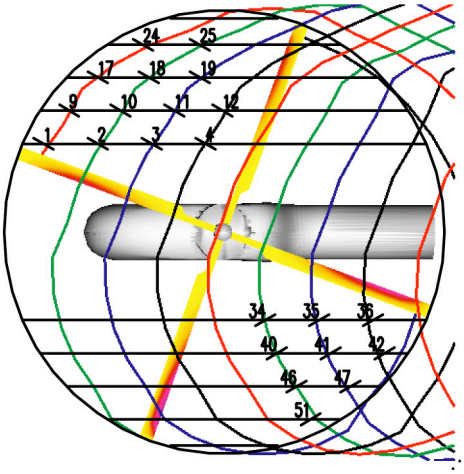

a) rotor position where the reference blade in the first quadrant is at ψ = 70°.

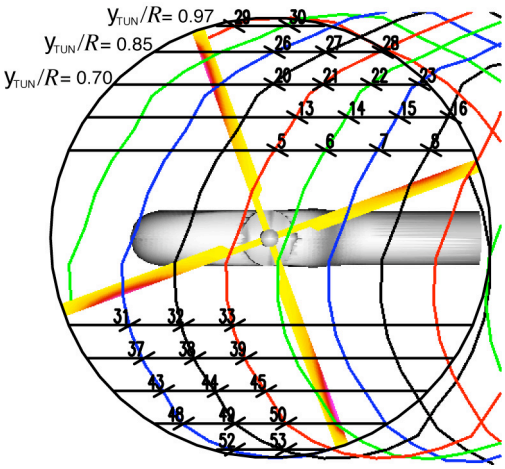

b.) rotor position where the reference blade in the first quadrant is at ψ = 20°.

Figure 2. Schematic showing the (cut-plane) locations of the 3-C PIV rotor wake measurements for two different reference blade positions.

PIV data and presentation

The PIV images were processed with interrogation window sizes of 24x24 pixels, which results in a resolution (grid spacing) of 0.00154 m/vector. Velocity vector fields were obtained from each PIV image-pair using the cross-correlation method (Refs. 22 and 24).

Figure 3 illustrates the view orientation of the PIV cut planes (of Fig. 2), presented in the paper. The view, as well as each cut-plane is orientated 30.7° from the

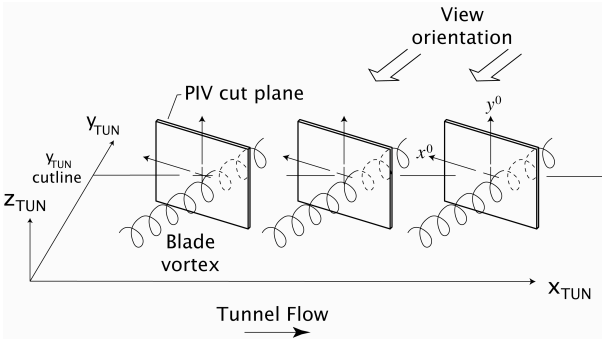

Figure 3. Illustration of the view orientation of PIV cut planes presented in figures to follow for the advancing side of the rotor.

tunnel axis. The image frames, which coincide with the cut planes, are defined with coordinates (x^0, y^0), where y^0 is aligned with the z_{TUN} axis. The frames are in rows such that the y^0 axis cuts through the same y_{TUN} axis value. For the present advancing side cuts, the PIV cameras were on the positive y_{TUN} side, out of the flow. In the present paper, processed results are given for PIV cut planes on the advancing side along y_{TUN}/R = 0.70, 0.85, and 0.97 only (see Fig. 2).

VORTEX WAKE DEFINITION

The rotor wake contains vortices that are forming, ones that are well formed, and ones that have been burst or involved in blade vortex interactions (direct or near misses). The out-of-plane component of vorticity, $\omega_{z^0} = \left(\partial v/\partial x - \partial u/\partial y\right)^0$ is employed to identify the vortex within a given PIV map. The Δx and Δy correspond to the PIV grid spacing. Vorticity distributions, unlike velocity presentations, are independent of the choice of any mean velocity values. Figure 4 shows the vorticity distribution of PIV measurements at two different streamwise locations along y_{TUN}/R=0.70. Figure 5 shows the same for y_{TUN}/R=0.85.

The vorticity distributions of the wake at the most upstream locations are shown in Figs. 4(a) and 5(a). These distributions clearly reveal vortex sheets being rolled around a center, indicating the vortex is still under formation and in its early stages of the roll-up process. For the more downstream locations, in Figs. 4(b) and 5(b), the vortex is more evolved, with a core region well defined. It is interesting to note that for Fig. 4(b), the vortex is not as tightly formed as that shown in Fig. 5(b). From examination of PIV measurements at

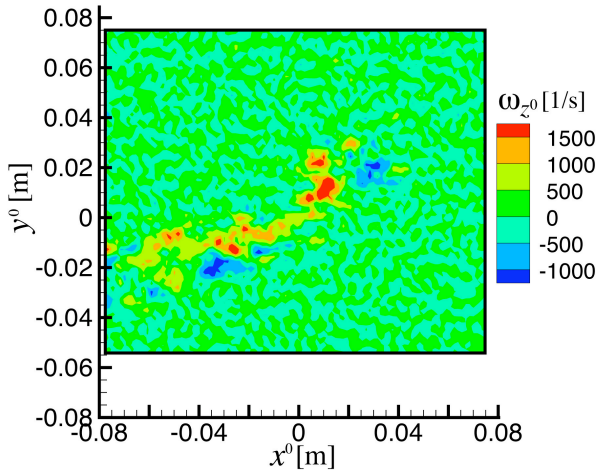

a) cut #17, image #7, *CV*=(0.0052, 0.0102) m ,x_{TUN}= -1.19m.

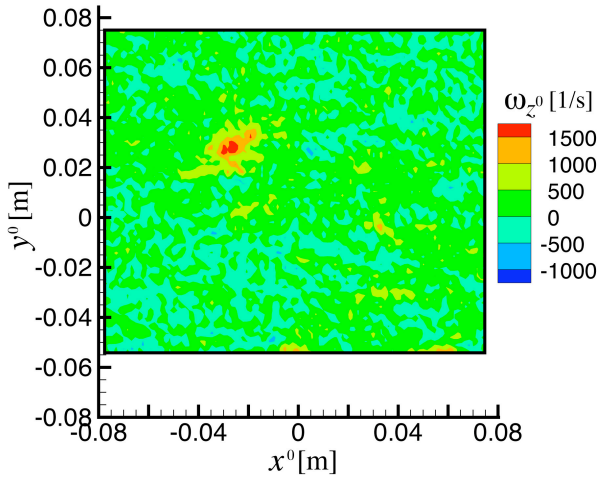

b) cut #22, image #8, *CV*=(-0.0267, 0.0282) m, x_{TUN}=1.36m.

Figure 4. Vorticity contours computed from instantaneous PIV images measured on the advancing side, y_{TUN}/R=0.70.

PIV cut-planes #18-#21, a blade appears (Ref. 19) to have passed (and interacted) closely with the wake, interrupting the roll-up of the tip vortex of Fig. 4(b). This was not found in the measurements taken along y_{TUN}/R=0.85 (Fig. 5(b)), where the vortex rolled up quickly and convected downstream without significant interference from passing blades.

To determine the vortex core size and strength the center of the vortex must first be identified. The center of vorticity is used to define the vortex center (Ref. 19). The center of vorticity is defined as

$$CV = \sum_k (\omega_z)_k \cdot (x_k, y_k) / \sum_k (\omega_z)_k \qquad (1)$$

where k are grid point indices taken over the whole PIV

image. For most cut-planes, not all 100 instantaneous images have *CV* positions determined. Excluded are images where the maximum values of ω_z do not exceed a 20 % threshold of the maximum ω_z, found by considering all 100 image frames. This eliminates extraneous images where seeding, laser light, other PIV conditions, or an occasional vortex-formation disruption produced ill-defined vortices. For majority of cut-planes 5 or less frames were excluded. Figure 6 shows an instantaneous vortex image with the *CV* position determined by the use of Eq. (1).

Once the center of the vortex is known the core size can be determined. A common method for determining this is to take horizontal and vertical velocity cuts through the center of the vortex. Example

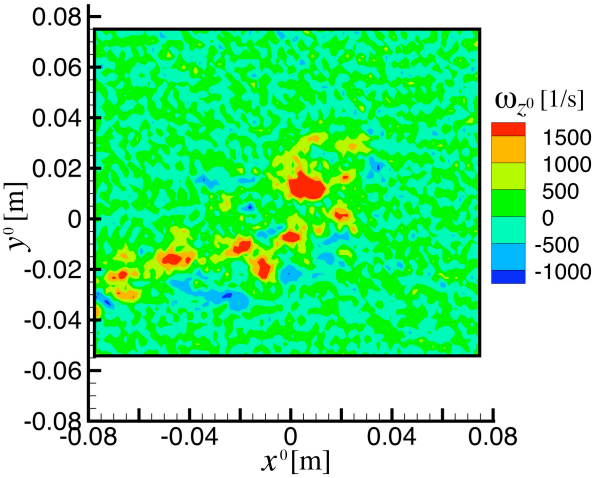

a) cut #24, image #10, *CV*=(0.0065, 0.0130)m, x_{TUN} = - 0.75m.

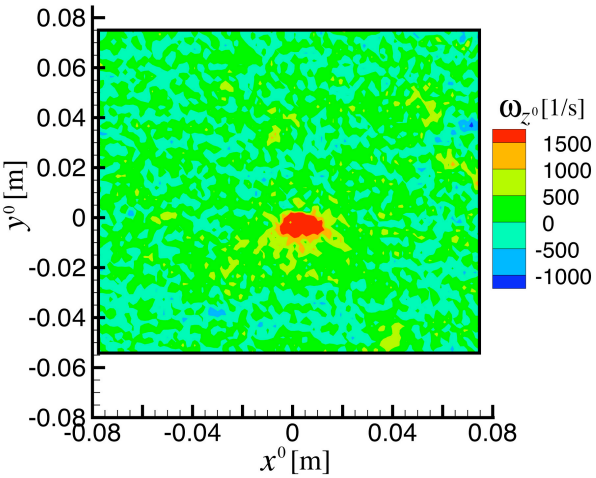

b) cut #27, image #3, *CV*=(-.00269, 0.0097) m, x_{TUN} =0.76m.

Figure 5. Vorticity contours as per caption as Fig. 4, but with y_{TUN}/R=0.85.

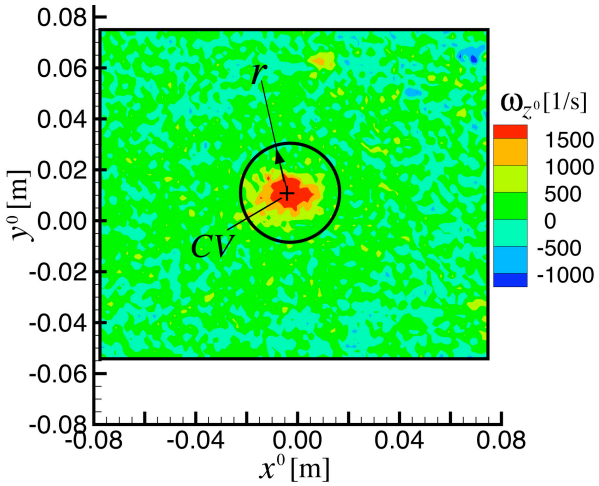

Figure 6. Vorticity contours from cut #28, (y_{TUN}/R=0.85). Also shown are the center of vorticity (*CV*) and the "integration disk" of radius *r* used to determine circulation Γ.

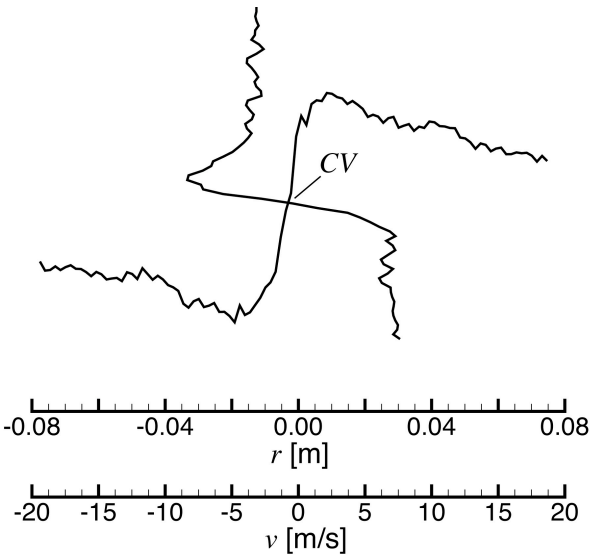

Figure 7. Vertical and horizontal velocity cuts through the vortex center (i.e. center of vorticity, *CV*= -0.00296m, 0.01099m) shown in Fig. 6.

plots of these are shown in Fig. 7 for the vortex shown in Fig. 6. The core circumferential velocity v_C is 1/2 the difference in peak velocities across the vortex, and the associated core radius r_C is 1/2 the distance between the locations of these peak velocities. For Fig. 7, (r_C, v_C)=(0.014m, 9.4m/s) from the horizontal cut and (r_C, v_C)=(0.0092m, 7.8m/s) from the vertical cut. The r_C from the horizontal cut is about twice as large as that from the vertical cut. One might argue that this is because the vortex is skewed with respect to the PIV cut window, thus giving the appearance of an oval cross

section. Then the average of the two results would give a reasonable value of the vortex core size, but the ragged character of the instantaneous image cuts also gives uncertainty to "true accuracy" of the choice of r_C and v_C. The magnitude of v_C is always biased to higher values. Averaging of velocity cuts would smooth out the ragged character, but, the results would still be biased because individual vortices of different sizes would tend to smear and flatten upon averaging – even if centered (Ref.19).

A method which uses vorticity distributions, instead of operating on limited velocity cuts distributions has been shown to be better based statistically, have less bias, and in a form that renders a more complete description of the vortices. This method is known as the "vorticity disk" method (Ref. 19). The *CV* position is shown in Fig. 6, along with a radius r defining a circle (or disk) that encloses vorticity. The procedure of the "disk" method is to first integrate (both positive and negative) vorticity over areas within succeeding values of radius r, to render circulation Γ as a function of r. The result of this integration is shown in Fig. 8 (a). Using the relationship $v = \Gamma/2\pi r$, one obtains Fig. 8 (b), where r_C is chosen at the maximum value of v (designated as v_C, $v_C = \Gamma_C/2\pi r_C$). Here, this method gives (r_C, v_C) = (0.0104m, 7.71m/s), which is deemed to be a more accurate measure of the vortex than that found above using the two cut procedure of Fig. 7 (a) and then averaging the two results.

The "vorticity disk" method as with other methods is limited, in that it intrinsically assumes that the vortex tube is aligned normal to the cut plane. Errors associated with the vortex orientation with respect to the PIV window can affect defining vortex parameters, such as core size (biased towards indicating a larger core size) and strength (peak velocity). As previously indicated, and will be shown, the orientation angles can be on the order of 45 degrees.

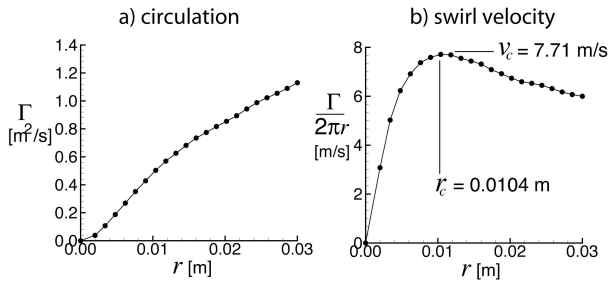

Figure 8. Vortex parameters determined by the "voticity disk" method for the vortex shown in Fig. 6.

CUT-PLANE TILT ANALYSIS

In this paper, two analysis approaches are used on processed three-component velocity data defined at grid points over the PIV cut-planes. The approaches use different components of the velocity field (with different criteria) in order to independently define the vortex axis orientation. For a perfectly defined vortex, the determined orientations should be identical. Given an orientation, the velocity data is projected to an "ideal" cut-plane (normal to the vortex axis) where one can properly determine key vortex parameters. Here, a basic vortex model and orientation geometry is first defined. The axial-velocity model and spin-velocity model are then defined.

Basic Vortex Tilt Model

Figure 9 shows the vortex tube model used in the tilt-plane analyses of the present paper. The radius of the tube is r_C with circulation Γ and corresponding circumferential or spin velocity v_C. The tube also has an axial flow of velocity magnitude U_{AX}. The PIV cut-plane is defined $z^0 = 0$ in the $s^0 = (x^0, y^0, z^0)$ coordinate system. The tube is centered on the s^0 coordinate system, but tilted at Θ_0 with respect to the z^0 axis. The orientation angle on the cut-plane with respect to the x^0 axis is Φ_0. The vortex tube has its own coordinate system $s^\ell = (x^\ell, y^\ell, z^\ell)$ with z^ℓ defining the center axis of the vortex tube. The plane

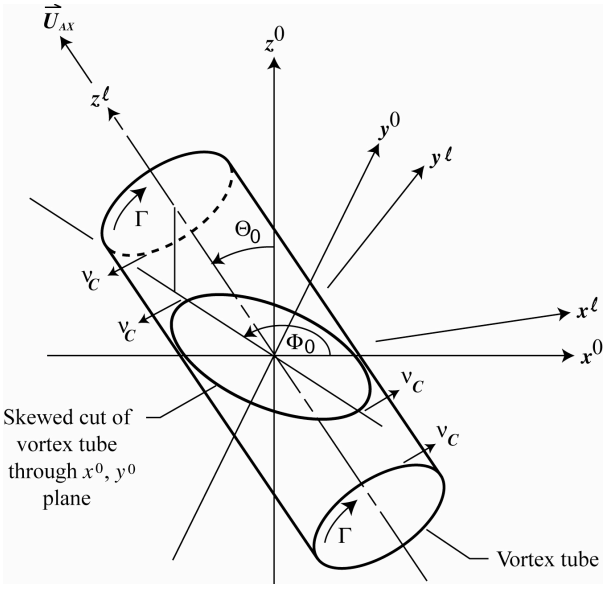

Figure 9. Schematic of vortex tube tilted with respect to PIV cut-plane through vortex.

$(x^\ell, y^\ell, z^\ell = 0 \text{ or constant})$ is perpendicular to the tube axis and represents the desired normal cut-plane to the vortex.

The axial velocity component is written as a vector in the s^0 coordinate system as

$$\vec{U}^0_{AX} = U_{x^0}\hat{i} + U_{y^0}\hat{j} + U_{z^0}\hat{k} \qquad (1)$$

$$= U_{AX}(\cos\alpha_z\hat{i} + \cos\beta_z\hat{j} + \cos\gamma_z\hat{k}) \qquad (2)$$

where $U_{AX} = \left|\vec{U}^0_{AX}\right|$ and the directional cosines $\cos\alpha_z$, $\cos\beta_z$, and $\cos\gamma_z$ are

$$\begin{aligned}\cos\alpha_z &= \cos\alpha_{x^0 z^\ell}\\ \cos\beta_z &= \cos\alpha_{y^0 z^\ell}\\ \cos\gamma_z &= \cos\alpha_{z^0 z^\ell}\end{aligned} \qquad (3)$$

where $\alpha_{x^0 z^\ell}$, $\alpha_{y^0 z^\ell}$, and $\alpha_{z^0 z^\ell}$ are the angles from the axes x^0, y^0, and z^0 to the axis z^ℓ, respectively. The relationship between the coordinate systems is

$$s^0 = \Pi^{0\ell} s^\ell \text{ and } s^\ell = \Pi^{\ell 0} s^0 \qquad (4)$$

with $\Pi^{0\ell}\Pi^{\ell 0} = \Pi^{\ell 0}\Pi^{0\ell}$, $\Pi^{0\ell} = (\Pi^{\ell 0})^T = (\Pi^{\ell 0})^{-1}$. The matrix

$$\Pi^{0\ell} = \begin{bmatrix}\cos\alpha_x & \cos\beta_y & \cos\gamma_z\\ \cos\alpha_x & \cos\beta_y & \cos\gamma_z\\ \cos\alpha_x & \cos\beta_y & \cos\gamma_z\end{bmatrix} \qquad (5)$$

contains the direction cosines for each combination of s^0 and s^ℓ axes (Ref. 25). For the case of unit direction with $\vec{U}_{AX}$ aligned along z^ℓ, we obtain $s^0 = \Pi^{0\ell}\cdot(s^\ell = col(0,0,1)) = col(\cos\alpha_z, \cos\beta_z, \cos\gamma_z))$. With this relationship and the knowledge that only rotations about the x^0 and y^0 axes are needed to define s^ℓ, one can determine $\Pi^{0\ell}$ and thus $\Pi^{\ell 0}$. By Eq. (4), one can map velocity values over the PIV cut-plane of s^0 to the "vortex normal" cut-plane of s^ℓ. The relationship $s^\ell = \Pi^{\ell 0}\cdot(s^0 = col(x^0, y^0, 0))$ renders corresponding (x^ℓ, y^ℓ) grid points. The velocities there are

$$\vec{U}^\ell = \begin{bmatrix}U_{x^\ell}\\ U_{y^\ell}\\ U_{z^\ell}\end{bmatrix} = \Pi^{\ell 0}\cdot\begin{bmatrix}U_{x^0}\\ U_{y^0}\\ U_{z^0}\end{bmatrix} \qquad (6)$$

Axial-Velocity Model

The axial-velocity model processing uses the velocity measurements in the PIV cut-plane to define the axial flow field through the vortex core. Figure 10(a) illustrates 3-component velocity vectors defined over a number of k grid points over the vortex region. We define Region *A* as the area within a predetermined radius r_C. Region B is that area beyond r_C but within $2\,r_C$. Regions A and B contain K_A and K_B grid points, respectively. It is assumed that Region *A* contains the axial flow within the vortex core, as well as a mean convection velocity for the vortex in general. Region *B* should contain mostly this mean convection and spin components. (The spin velocities in both Regions *A* and *B*, would not contribute to the mean values.) Therefore, isolating the convective flow, the average through Region *B* is

$$\vec{U}^0_{AVG\_B} = [\sum_k U_{x^0}(x_k, y_k)\hat{i} + \sum_k U_{y^0}(x_k, y_k)\hat{j} + \sum_k U_{z^0}(x_k, y_k)\hat{k}]_B / K_B \qquad (7)$$

The vector field obtained by subtracting this from region *A* and *B* is illustrated in Figure 10(b). The mean of the resultant field over Region *A* is taken as the mean resultant axial velocity represented in Eq. (1), which is

$$\vec{U}^0_{AX} = \vec{U}^0_{AVG\_A} - \vec{U}^0_{AVG\_B} \qquad (8)$$

with $\vec{U}^0_{AVG\_A}$ defined the same as Eq. (7) with A replacing B. This permits the solution of the tilt plane per Eqs. (1)-(6), for each PIV image sample.

Spin-Velocity Model

The intention of the Spin-velocity model is to isolate the vortex rotation, rather than the axial flow, to defining the orientation of the vortex. Figure 11(a) shows, similar to the illustration of Fig. 10(a), the velocity field defined over the PIV cut-plane. The region (call this Region *C*) shown is within a circle with a radius on the order of r_C (actually $1.2\,r_C$ is used).

With the subtraction of the mean $\vec{U}^0_{AVG\_C}$ (defined as above) over this Region *C*, the resultant velocity field $\vec{u}^0$ is

$$\vec{u}^0 = \vec{U}^0 - \vec{U}^0_{AVG\_C} \qquad (9)$$

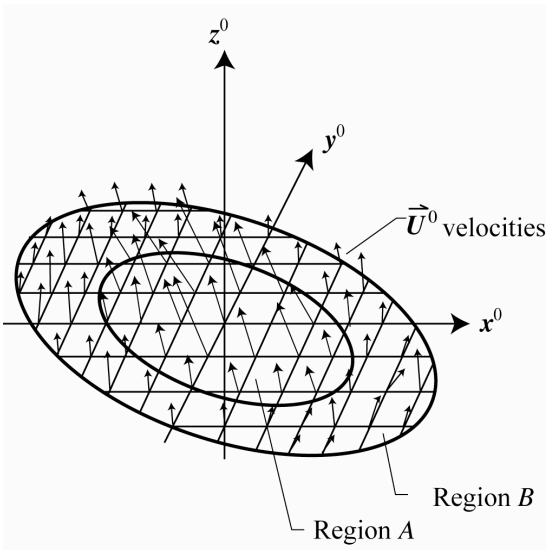

(a) Raw velocities over grid points over two regions

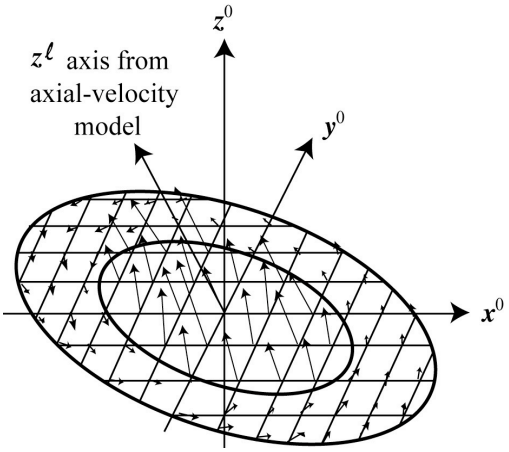

(b) Velocities with mean over Region B subtracted from all

Figure 10. Velocity vectors over PIV cut-plane used to determine mean core axial flow $\vec{U}^0_{AX}$ through vortex per Axial-velocity model.

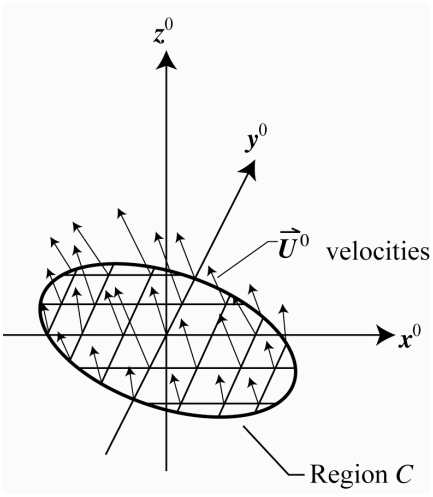

(a) Raw velocities over grid points over vortex core region

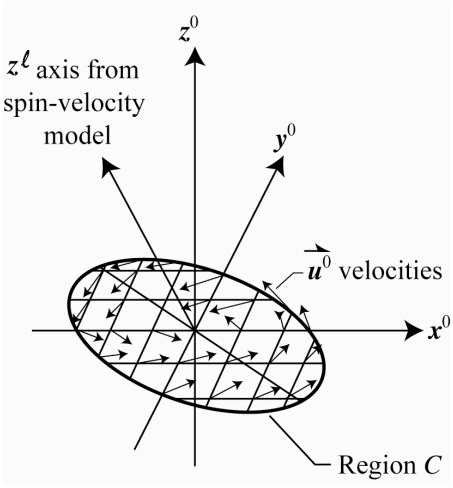

(b) Velocities with mean velocity subtracted

Figure 11. Velocity vectors over region of PIV cut-plane used in the Spin-velocity model for determining vortex orientation.

An illustration of $\vec{u}^0 = \vec{u}^0(x^0, y^0)$ is shown in Fig. 11(b), where the spin about the vortex center at the origin is apparent. Note, of course, that $\oint_C \vec{u}^0 \cdot d\vec{k} = 0$.

Figure 12 shows the resultant velocity components at a position $\vec{r} = (x^0\hat{i} + y^0\hat{j})$. The component of velocity in the plane normal to $\vec{r}$ is

$$u_\perp = \left(\frac{\vec{r}}{|\vec{r}|} \times \hat{k}\right) \cdot \vec{u}^0 \qquad (10)$$

With the up-wash component of velocity being u_{z^0}, the up-wash angle through the (x^0, y^0) plane is

$$\tan\Phi = u_{z^0} / u_\perp \qquad (11)$$

With this relationship, one determines Φ for each grid point location and obtains a plot like Fig. 13. This shows measured data (cut-plane #28, seq. #3) processed using Eq. (11). The data is first fit with a tensor product spline (Ref. 26), shown as the red curve in Fig. 13. This smoothes out irregularities in a least squares sense, and resolves multi-values of Φ. The green curve

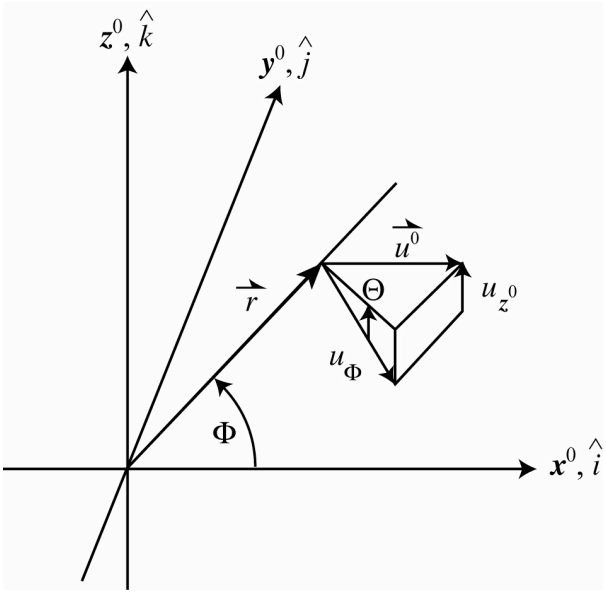

Figure 12. Resultant velocity components (from Eq. (9) or Fig. 11(b)) at a grid point for Spin-velocity model.

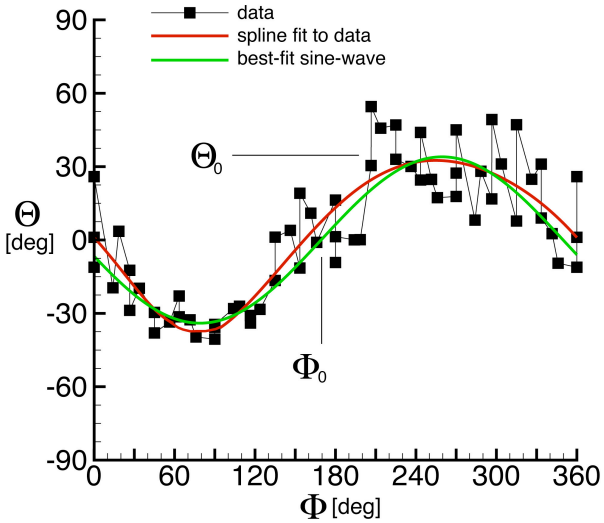

Figure 13. Up-wash angles Φ for grid points within the vortex core region (Region *C*). Best fit sine-wave curve used for defining vortex tilt is shown. Data from cut-plane #28, image #3, Θ_0=34^0, Φ_0=170^0.

through the data is a best-fit sine-wave of the form

$$\Theta = \Theta_0 \sin(\Phi - \Phi_0). \qquad (12)$$

The best-fit sin-wave curve is determined by cross-correlating a sine function of unit amplitude with the spline fit. The resulting cross correlation function is also a sine wave for which twice its amplitude is Θ_0 and Φ_0 is where it first intersects Φ = zero.

With Θ_0 and Φ_0 determined by this fit, two solutions for transformed axes are possible. One solution shown in Fig. 14 is a counter-clockwise vortex line (positive circulation Γ by standard right-hand rule) tilted by Θ_0 toward angle Φ_0. The other is a clockwise vortex line tilted by Θ_0 toward $\Phi_0 + \pi$. For the former,

$$\frac{\vec{U}^0_{AX}}{|\vec{U}^0_{AX}|} = (\ell_z\hat{i} + m_z\hat{j} + n_z\hat{k}) \qquad (13)$$
$$= (\sin\Theta_0 \cos\Phi_0\hat{i} + \sin\Theta_0 \sin\Phi_0\hat{j} + \cos\Theta_0\hat{k})$$

Equation 13, as with the Axial-velocity model, defines a solution of the tilt plane for each PIV cut-plane record.

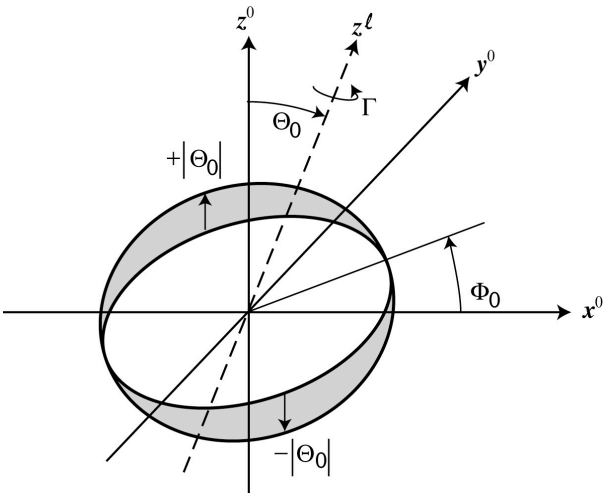

Figure 14. Up-wash angle ∏ distribution with respect to vortex axis tilt.

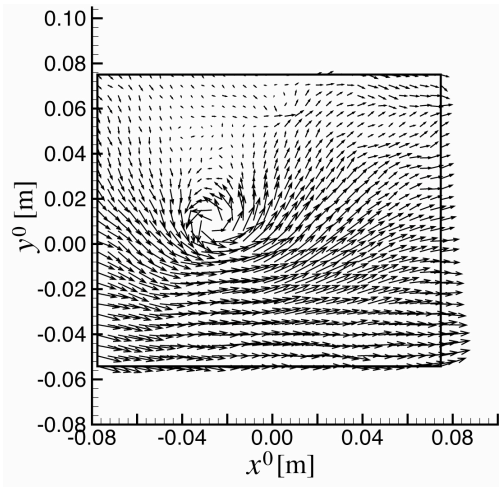

a) in-plane velocity components (u_{x^0} , u_{y^0}) distribution.

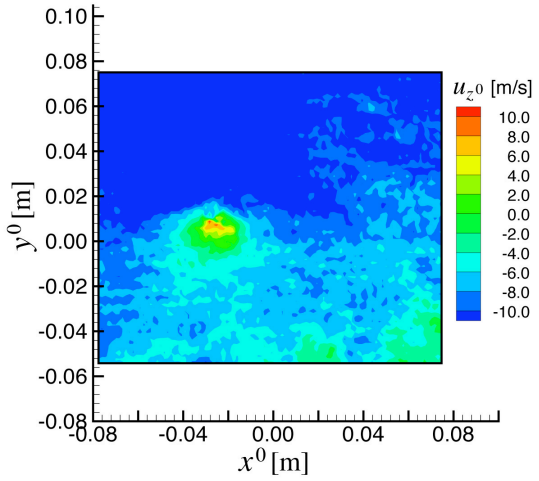

b) out-of-plane velocity component (u_{z^0}) distribution.

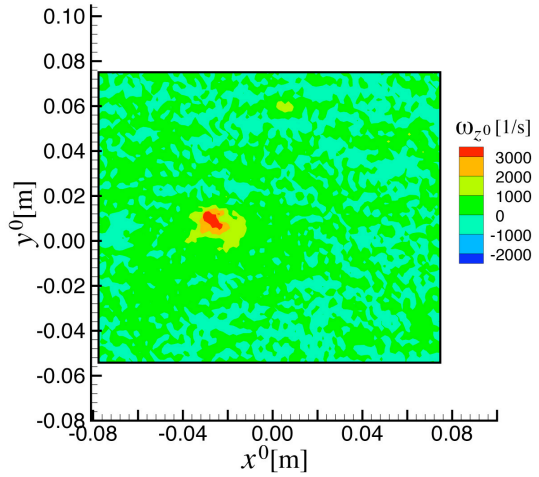

c) vorticity distribution

Figure 15. Velocity vector and vorticity distributions for a vortex at PIV cut-plane location #28, y_{TUN}/R=0.85.Image#3

RESULTS

PIV Image Re-orientation

For PIV cut-plane location #28, Fig. 15 shows instantaneous distributions of in-plane velocity vectors, out-of-plane velocity components, and vorticity for a well-developed vortex. The vortex is older than that for Fig. 5(b) by an amount corresponding to 90 deg. of rotor rotation. For the velocity presentations, the mean velocity $\vec{U}^0_{AVG\,B}$ obtained by Eq. (7) was subtracted to better reveal the vortex features. It is seen that the vortex cut is non-normal as suggested by its horizontally-elongated appearance. Using the Spin-velocity model detailed in the last section, the tilt angle of $\,_0$=34 deg. and the tilt-alignment angle of $\,_0$=170 deg. was found and the axes and velocities were rotated to render Fig. 16, the corresponding results for the "vortex normal" cut-plane projection for velocity distribution. (Note that the shape of the cut-plane projection is a parallelogram whose shape depends on $\,_0$ and $\,_0$.) It is seen that the vortex velocity fields now appears rounder. The vorticity distribution has been recalculated using the new velocity distribution and is given in Fig. 16(c). Using the Axial-velocity model, it was found that $\,_0$=32 deg. and $\,_0$=184 deg. which is close to that of the Spin-velocity model in Fig. 16. Using these numbers produces very similar results as that of Fig. 16, and is thus not shown. By employing the previously discussed "vorticity disk"

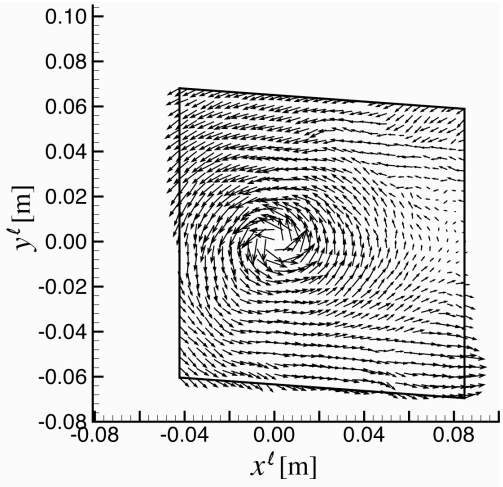

a) in-plane velocity components (u_{x^ℓ} , u_{y^ℓ}).

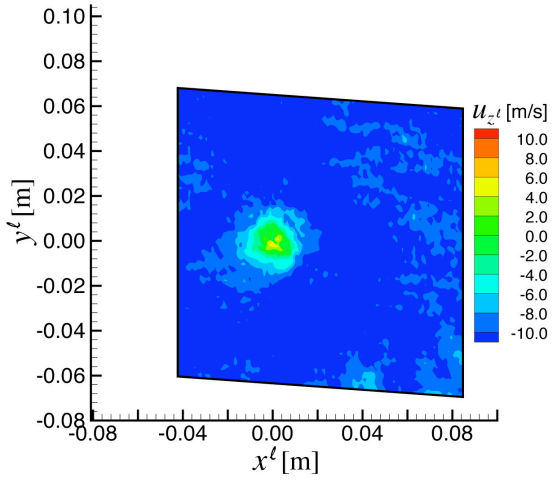

b) out-of-plane velocity component (u_{z^ℓ}) distribution.

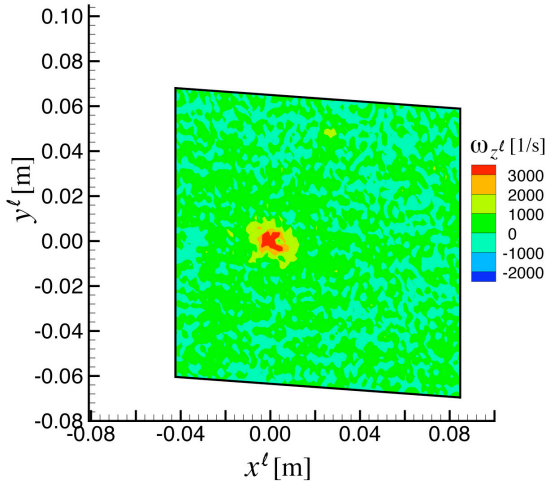

c) vorticity distribution

Figure 16. Spin-velocity method applied to measured PIV data of Fig. 17 (cut-plane location #28, y_{TUN}/R=0.85)

method, the original data of Figure 15 renders values of (r_C , v_C , U_{AX}) = (0.0090m, 9.34m/s, 2.92m/s), whereas using the cut-plane projection data of Fig. 16 gives the "corrected" values of (r_C , v_C , U_{AX}) = (0.0076m, 10.35m/s, 3.87m/s).

Instantaneous and Averaged Vortex Orientations

Figure 17 shows the calculated tilt angle Φ_0 and tilt-alignment angle Θ_0 values for the complete set of instantaneous PIV cut-plane at three x_{TUN} locations along y_{TUN}/R = 0.70. Figure 18 shows the Φ_0 and Θ_0 results for three x_{TUN} locations further outboard along y_{TUN}/R = 0.85. The cut-plane projection of Fig. 16 was accomplished using the Φ_0 and Θ_0 values for the third image-frame of Fig. 18(c). The figures show that using

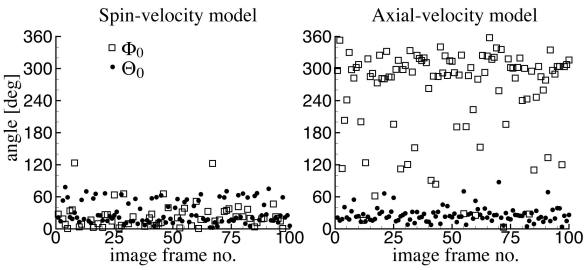

a) cut-plane #17, x_{TUN}= -1.19m.

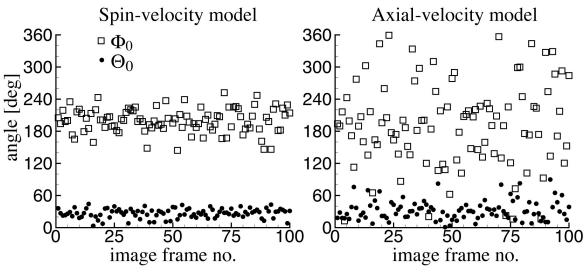

b) cut-plane #21, x_{TUN}= 0.73m.

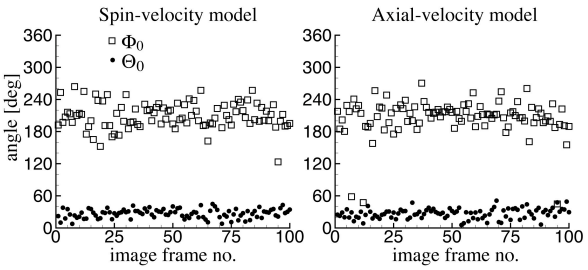

c) cut-plane #22, x_{TUN}= 1.36m.

Figure 17. Tilt angle and tilt-alignment angle vs image frame number for different cut-planes along y_{TUN}/R=0.70.

the Spin-velocity model gives more stable values (less scatter) of Φ_0 and Θ_0. The Axial-velocity method tends to have significant scatter, in part due to the small magnitude of the axial velocity component (magnitudes are subsequently shown). When U_{AX} is substantial the scatter is significantly decreased as shown in Figs. 17(c) and 18(c). If the vortex position were invariant there would be no scatter. The fact that there is scatter is also an indication that there is uncertainty in the position and orientation of the vortices.

Figures 19, 20, and 21 show the averaged values of Φ_0 and Θ_0 at different cut-plane locations along y_{TUN}/R = 0.70, 0.85, and 0.97, respectively. The associated standard deviations of Φ_0 and Θ_0 are shown in Figs. 22, 23, and 24, respectively. Where vortices are mature and well developed, both methods determine values of Φ_0 and Θ_0 that generally match. This means that the ideal vortex tube model illustrated in Fig. 9 appears to be appropriate for describing the more mature vortices. The resultant values (Φ_0 and Θ_0) are

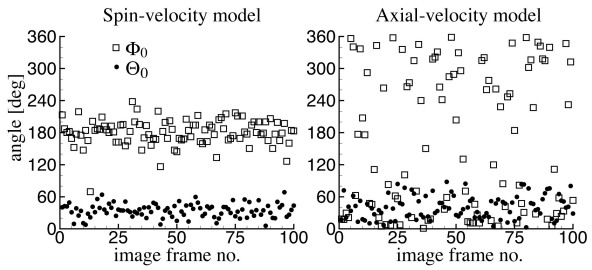

a) cut-plane #24, x_{TUN}= -0.75m.

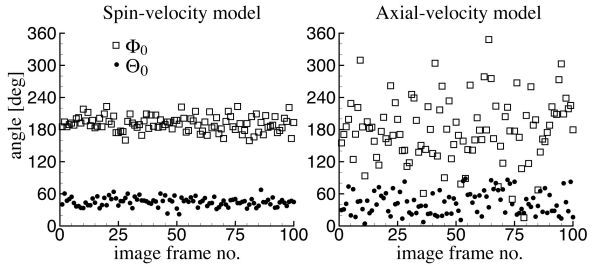

b) cut-plane #25, x_{TUN}= -0.22m.

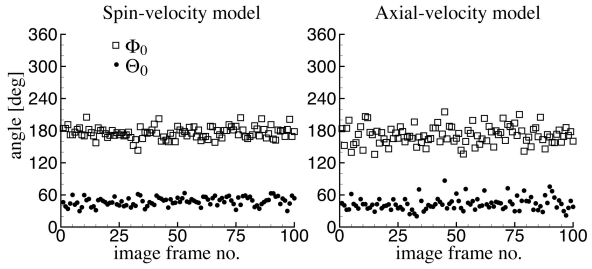

c) cut-plane #28, x_{TUN}= 1.34m.

Figure 18. Same caption as Fig. 17, except y_{TUN}/R=0.85.

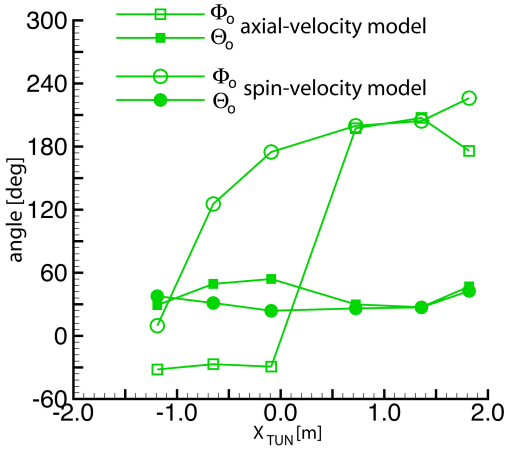

Figure 19. Averaged tilt angles and tilt-alignment angles for vortices along y_{TUN}/R=0.70,

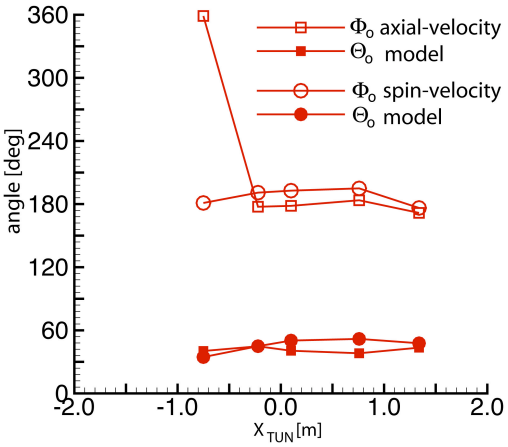

Figure 20. Averaged tilt angles and tilt-alignment angles for vortices along y_{TUN}/R=0.85.

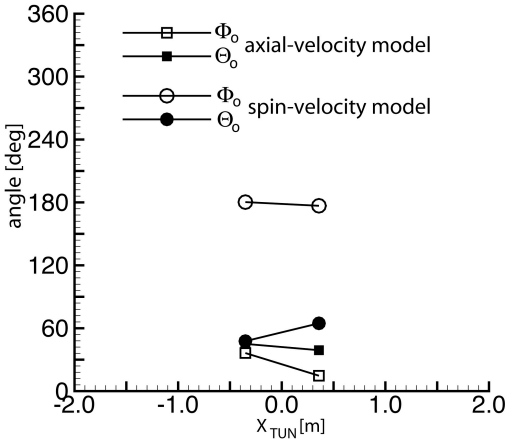

Figure 21. Averaged tilt angles and tilt-alignment angles for vortices along y_{TUN}/R=0.97.

consistent with pre-test calculations, such as those illustrated in Fig. 2, that show the vortices examined here to be tilted on the order of 45° (30° to 60°) from the normal to the PIV cut-planes, and aligned in the aft (180°) direction. Also, as expected, the determined values of Φ_0 increase for increasing y_{TUN}/R (= 0.70 to 0.97) locations.

At early vortex formation stages (at larger negative x_{TUN} locations), the methods can give differing values of Φ_0 and Θ_0. For the vortices along y_{TUN}/R=0.70, the formation stage extends into positive x_{TUN} locations, whereas for the vortices along the larger y_{TUN}/R of 0.85 and 0.75, the vortices are known to roll-up and be fairly well defined by the first cut-plane location (Ref. 19). The vortices' spin velocity tends to be significant. The relative magnitude of the axial velocity is (as will be shown) significantly smaller and is believed to be part of the reason for the large scatter seen for the Axial-velocity model.

The standard deviations shown in Figs. 22, 23, and 24 provide an indication of how stable the computed orientation angles are for a given set of images. Where both orientation models give the same standard deviation as well as actual values, the vortices are well developed and defined, i.e. not burst or under formation. In Fig. 23 for y_{TUN}/R=0.85, the standard deviation for the Axial-velocity model steadily decreases with increasing x_{TUN} to be that of the Spin-velocity model. The axial velocity (to be subsequently shown) steadily increases thus stabilizing and decreasing the scatter in the computed values. The actual values of Φ_0 and Θ_0 for this y_{TUN}/R=0.85 are shown in Fig. 20. The results from both methods compare well except at the most positive x_{TUN} location, where the vortex roll-up process is clearly visible in Fig. 5(a). For the vortices along y_{TUN}/R=0.70, the values and standard deviation of Φ_0 (Figs. 19 and 22) from the two models differ significantly. As noted earlier, the vortices are under formation or in close interaction with the rotor blades until approximately x_{TUN}=1.4m. The large differences in the results from the two methods indicate that at these locations the vortices are not well represented as vortex tube.

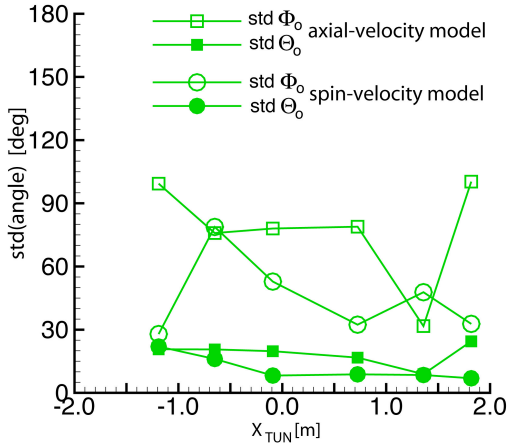

Figure 22. Standard deviation of the average tilt angles and tilt-alignment angles for vortices along y_{TUN}/R=0.70.

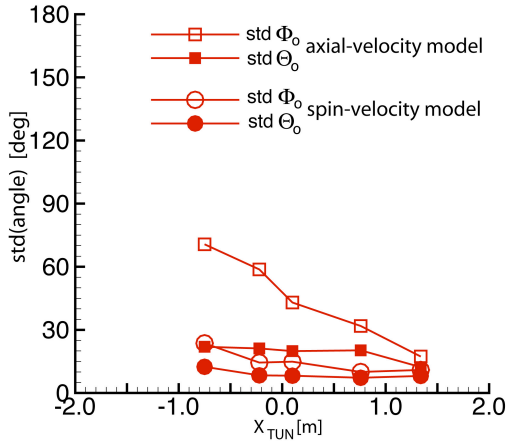

Figure 23. Standard deviation of the average tilt angles and tilt-alignment angles for vortices along y_{TUN}/R=0.85.

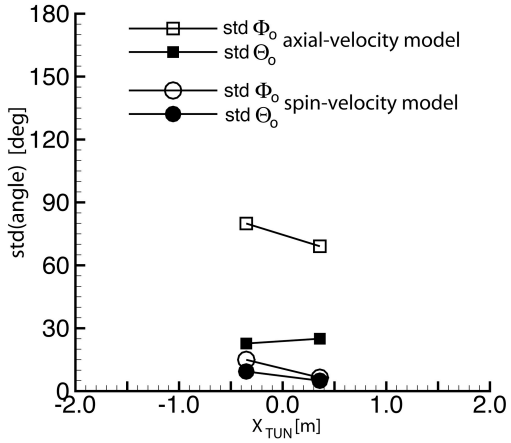

Figure 24. Standard deviation of the average tilt angles and tilt-alignment angles for vortices along y_{TUN}/R=0.97.

Vortex Parameter Comparisons

Figures 25, 26, and 27 show, respectively, the key vortex parameters of average vortex core radius r_C, normalized with rotor radius, average spin velocity v_C at r_C, normalized by rotor (hover) tip speed, and average core axial velocity U_{AX}, also normalized by tip speed. The results are presented as a function of streamwise distance for each of our y_{TUN}/R stations. The r_C and v_C parameters were determined using the vorticity disk method for each instantaneous PIV cut-plane velocity distribution and then averaged. For each PIV cut-plane image frame record, the orientations were uncorrected and corrected, alternately, by the Axial-velocity and Spin-velocity methods. (The procedure did not employ the averaged Ω_0 and Ω_0 values of Figs. 19, 20, and 21.) The U_{AX} values were determined from the use of the Spin-velocity method to reorient the instantaneous cut-planes and to use Eq. 8.

The "uncorrected" values of r_C and v_C correspond to values determined in Ref. 19. (The axial velocity U_{AX} was not studied in Ref. 19.) The results for increasing values of x_{TUN} for the different spanwise y_{TUN} axes represent roughly the evolution of the same vortex segment as it travels downstream. With the tendency to maintain the same vortex strength in their travel downstream, increased r_C is seen to match with decreased v_C, and vice versa. The three different vortex segments have differing strengths, of course, dependent on loading over the blade at its upstream position. A key result here is that there are differences in the corrected and uncorrected values. As expected, the corrected r_C values are always smaller (with one exception) by about 10 to 20%. The corrected v_C values are generally larger (always larger for the Spin-velocity method). It is believed that in most cases the Spin-velocity method is the preferable method because of both the lower uncertainty (scatter) of results and the stronger spin velocities (better "signal-to-noise") compared to the axial velocities. The effects are

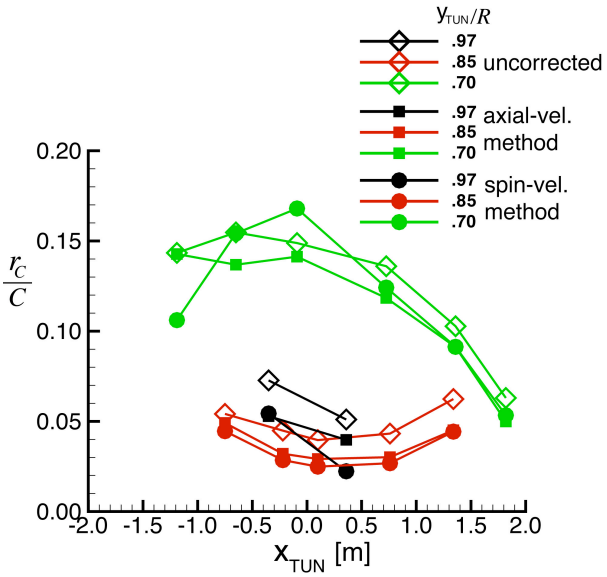

Figure 25. Core size (r_C) vs x_{TUN} determined from PIV maps that have been corrected for orientation compared to uncorrected results.

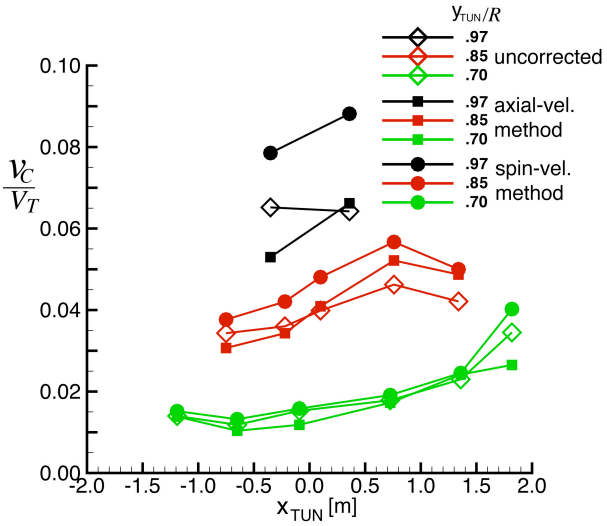

Figure 26. Maximum vortex core spin velocity determined from PIV maps that have been corrected for orientation compared to uncorrected results.

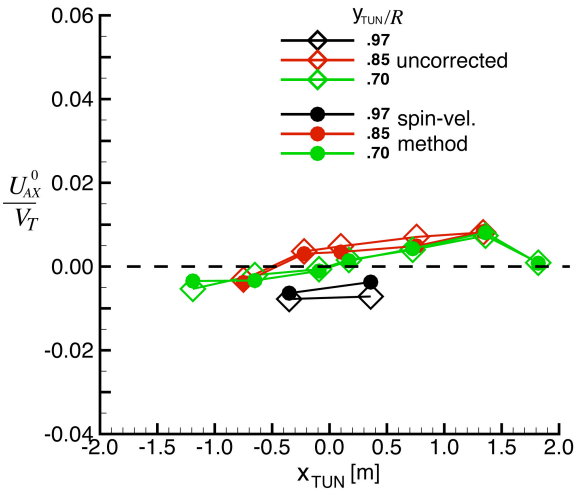

Figure 27. Vortex axial core velocity determined from PIV maps that have been corrected for orientation and compared to uncorrected results.

coupled, of course. Note that the v_C values in Fig. 26 can be on the order of 10 times or more than those of U_{AX} in Fig. 27. Actually, U_{AX} passes from negative to positive values. The low velocities can present a problem in extracting them accurately from the background flow field.

The observed cross-over from negative to positive values for U_{AX} is a noteworthy result (although perhaps peripheral) of this study. Negative U_{AX} means that the vortex axial-flow is directed toward the blade that released the vortex. This is the drag related axial flow and denoted as "wake-like" by Batchelor, (Ref. 27). Positive U_{AX} means that the axial flow is directed away from the blade that created the vortex. This is denoted as axial "jet-like" flow (Ref. 27). Experimental studies have reported both "wake-like" (Refs. 28, 29, 30) and "jet-like" (Refs. 15, 28, 29, 31) axial flows. The source of "jet-like" flow is related to the magnitude of the wing loading (Ref. 15, 28, 30), and has recently been shown related to a streamwise component of downwash directed along the trailing vortex axis (Ref. 28). The present results show a cross-over which represents the transition between the two axial flow types as the vortices mature and convect downstream. The drop in U_{AX} amplitude to near zero far downstream for y_{TUN}/R = 0.70 is believed to be due to the vortex bursting due to a near BVI, thereby interrupting the vortex evolution. The all-negative axial flow results for y_{TUN}/R = 0.97, may be an indication of the young age of the vortices measured.

CONCLUSIONS

In this study, two analysis methods are successfully developed to determine the orientation of vortex axes and to reorient the measured 3C-PIV velocity distribution maps (by re-orientation of axes and projection). The processing methods utilize the measured velocity components to create velocity distributions that one would have if the chosen PIV cut-plane were normal to the cut vortex axes. This is shown to permit the more accurate determination of vortex parameters important for the prediction of rotorcraft noise. The results presented are believed to provide the basis for better understanding of the structure of rotor wake vortices.

REFERENCES

1) Schmitz, F. H., "Rotor Noise", *Aeroacoustics of Flight Vehicles, Theory and Practice*, *Vol. 1, Noise Sources*, edited by H. H. Hubbard, Acoustical Society of America, New York, 1995, pp. 65-149.

2) Boxwell, D. A., Schmitz, F. H., Splettstoesser, W. R., Schultz, K. J., "Helicopter Model Rotor-Blade Vortex Interaction Impulsive Noise: Scalablity and Parametric Variations," *Journal of American Helicopter Society*, vol. 32, No. 1, 1987.

3) Brooks, T. F., Booth, E.R., Splettstoesser, W. R., Schultz, K. J., Kube, R., Niesel, G., and Streby, O., "Analysis of a Higher Harmonic Control Test to Reduce Blade Vortex Interaction Noise," *Journal of Aircraft*, Vol. 31, No. 6, Nov-Dec 1994, pp. 1341-1349.

4) Splettstoesser, W. R., Schultz, K. J., Kube, R., Brooks, T. F., Booth, E. R., Niesel, G., and Streby, O., "BVI Impulsive Noise Reduction by Higher Harmonic Pitch Control: Results of a Scaled Model Rotor Experiment in the DNW," presented at the 17th European Rotorcraft Forum, September 24-26, 1991, Berlin, Germany.

5) Brooks, T. F., Burley, C. L., "Rotor Broadband Noise Prediction with Comparison to Model Data,", AIAA Paper 01-2210, 7th AIAA/CEAS Aeroacoustics Conference, Maastricht, The Netherlands, May 2001.

6) Brezillon, J., Prieur, J., Rahier, G., "Investigation on Broadband Helicopter Rotor Noise,", AHS Technical Specialists' Meeting For Rotorcraft Acoustics and Aerodynamics, Williamsburg, Virginia, October 28-30, 1997.

7) Leishman, J. G., Baker, A., Coyne, A. J., "Measurements of Rotor Tip Vorticies Using Three-Component Laser Doppler Velocimetry, *Journal of the American Helicopter Society*, Vol. 41, No. 4, 1996.

8) Leishman, J. G., "Measurements of the Aperiodic Wake of a Hovering Rotor," *Experiments in Fluids*, vol. 25, 1998.

9) Han, Y. O., Leishman, J. G., Coyne, A., J., "Measurement of the Velocity and Turbulence Structure of a Rotor Tip Vortex," *AIAA Journal*, Vol. 35, No. 3, March 1997.

10) Coyne, A. J., Ghagwat, M. J., Leishman, J. G, "Investigation into the Rollup and Diffusion of Rotor Tip Vortices Using Laser Doppler Velocimetry," 53rd Annual American Helicopter Society Forum, May 1997.

11) Bhagwat, M. J., Leishman, J. G., "Generalized Viscous Vortex Model for Application to Free-Vortex Wake and Aeroacoustic Calculations," American Helicopter Society 58th Annual Forum, Montreal, Canada, June 11-13, 2002.

12) Bhagwat, M. J. and Leishman, J. G., "Correlation of Helicopter Rotor Tip Vortex Measurements," *AIAA Journal*, Vol. 38, No. 2, 2000, pp. 301-308.

13) Martin, P. B., Pugliese, G. J. and Leishman, J. G., "High Resolution Trailing Vortex Measurements in the Wake of a Hovering Rotor," American Helicopter Society 57th Annual Forum, Washington, D.C., May 9-11, 2001.

14) Mahalingam, R., and Komerath, N. M., "Characterization of the Near-Wake of a Helicopter Rotor", AIAA Paper 98-2909, 29th AIAA Fluid Dynamics Meeting, June 1998, Albuquerque, NM.

15) Mahalingam, R., and Komerath, N. M., " Measurements of the Near-Wake of a Helicopter Rotor in Forward Flight", AIAA Paper 98-0692, 36th AIAA Aerospace Sciences Meeting, January 1998, Reno, NV.

16) Heineck, J. T., Yamauchi, G. K., Wadcock, A. J., Lourenco, L., Abrego, A. I., "Application of Three-Component PIV to a Hovering Rotor Wake," American Helicopter Society 56th Annual Forum, Virginia Beach, Virginia, May 2-4, 2000.

17) McAlister, K. W., Tung, C., Heineck, J. T., "Forced Diffusion of Trailing Vorticity From a Hovering Rotor," American Helicopter Society 57th Annual Forum, Washington, D.C., May 9-11, 2001.

18) Raffel, M., Seelhorst, U., Willert, C., "Vortical Flow Structures at a Helicopter Rotor Model Measured by LDV and PIV," *The Aeronautical Journal*, Paper No. 2227, April 1998.

19) Burley, C. L., Brooks, T., F., van der Wall, B. G., Hugues, R., Raffel, M., Beaumier, P., Delrieux, Y., Lim, J., W., Yu, Y., Tung, C., Pengel., K ., Mercker, E., "Rotor Wake Vortex Definition – Initial Evaluation of 3-C PIV Results of the HART-II Study," 28th European Rotorcraft Forum, Bristol, UK, September, 17-20, 2002.

20) van der Wall, B. G, "Vortex Characteristics Analysed from HART Data," 23rd European Rotorcraft Forum, Dresden, Germany, 1997.

21) Yu, Y. H., Tung, C., van der Wall, B. G., Pausder, J., Burley, C. L., Brooks, T. F., Beaumier, P., Delrieux, Y., Mercker, E., Pengel, K., "The HART-II Test: Rotor Wakes and Aeroacoustics with Higher-Harmonic Pitch Control (HHC) Inputs – The Joint German / French / Dutch / US Project", American Helicopter Society 58th Annual Forum, Montreal, Canada, May 25-27, 2002.

22) Raffel, M., Richard, H., Schneider, G., Klinge, F., Ehrenfried, K., Pengel, K., Geenstra, G., "Recording and Evaluation Methods of PIV Investigations on a Helicopter Rotor Model," 11th International Symposium on Applications of Laser Techniques to Fluid Mechanics Lisbon, 8-11 July 2002.

23) van der Wall, B. G., Junker, B., Burley, C. L., Brooks, T. F., Yu, Y., Tung, C., Raffel, M., Hugues, R., Wagner, W., Mercker, E., Pengel., K., Holthusen, H., Beaumier, P., Delrieux, Y., "The HART II Test in the LLF of the DNW – A Major Step Towards Rotor Wake Understanding," 28th European Rotorcraft Forum, Bristol, UK, September, 17-20, 2002.

24) Richard, H., Raffel, M., "Rotor Wake Measurements: Full-scale and Model Tests," American Helicopter Society 58th Annual Forum, Montreal, Canada, May 25-27, 2002.

25) Tuma, J.J., *Engineering Mathematics Handbook*, McGraw-Hill Book Co., 1970, pp. 56-57.

26) De Boor, Carl, *A Practical Guide to Splines*, Springer-Verlag, New York, 1978.

27) Batchelor, G. K., "Axial Flow in Trailing Line Vorticies," Journal of Fluid Mechanics, Vol. 20, pp. 645-658, 1964.

28) Anderson, E. A., Lawton, T.A., "Effect of Wing Loading on Axial Velocity in a Wingtip Vortex," AIAA 2001-0578, Proceedings of the 39th AIAA Aerospace Sciences Meeting and Exhibit, January 2001.

29) Anderson, E. A., Wright, C. T., Lawton, T.A, "Experimental Study of the Structure of the Wingtip Vortex," AIAA 2000-0269, Proceedings of the 38th AIAA Aerospace Sciences Meeting and Exhibit, January 2000.

30) McAlister, K.W., Takahashi, R.K., "NACA0015 Wing Pressure and Trailing Vortex Measurements," NASA Technical Paper 3151, AVSCOM Technical Report 91-A-003, November 1991.

31) Devenport, W.J., Rife, M.C., Liapis, S.I., and Follin, G.J., "The Structure and Development of a Wing-Tip Vortex," Journal of fluid Mechanics, Vol. 312, pp. 67-106, 1996.